High Frequency Polar Waves in the Middle Atmosphere as seen in a Data Assimilation System

L. Coy *

E. O. Hulburt Center for Space Research, Naval Research Lab

Washington, District of Columbia

I. Stajner **A. M. DaSilva** **J. Joiner**

R. B. Rood

NASA Goddard Space Flight Center

Greenbelt, Maryland, USA.

*Corresponding author address: Lawrence Coy
E. O. Hulburt Center for Space Research, Naval Research Lab, Code 7646
4555 Overlook Avenue SW, Washington, DC 20375-5320, USA.
Tel: (202) 404-1266 , Fax: (202) 404-8090, e-mail: coy@uap2.nrl.navy.mil

ABSTRACT

This study examines the winter southern hemisphere vortex of 1998 using four times daily output from a data assimilation system to focus on the polar 2-day, wave number 2 component of the 4-day wave. The data assimilation system products are from a test version of the finite volume data assimilation system (fvDAS) being developed at Goddard Space Flight Center (GSFC) and include an ozone assimilation system. Results show that the polar 2-day wave dominates during July 1998 at 70°S. The 2-day wave is somewhat faster than 2 days during July 1998 with a period closer to 1.7 days and an average perturbation temperature amplitude for the month of over 2.5 K. The 2-day wave propagates more slowly that the zonal mean zonal wind, consistent with Rossby wave theory, and has EP flux divergence regions associated with regions of negative horizontal potential vorticity gradients, as expected from linear instability theory. Results for the assimilation produced ozone show that the 2-day wave represents a major source of ozone variation in this region. The ozone wave in the assimilation system is in good agreement with the wave seen in the POAM (Polar Ozone and Aerosol Measurement) ozone observations for the same time period. Some differences with linear instability theory are noted as well spectral peaks in the ozone field,

not seen in the temperature field, that may be a consequence of advection.

1. Introduction

The 4-day wave is a relatively common stratopause disturbance found mainly during the southern hemisphere winter. This high latitude wave consists of wave 1 and 2 (and some higher) components moving at nearly the same rotational period, about 3–4 days, so that the period of the wave 2 component is about 1.5–2 days. Many studies of the 4-day wave have focused on the wave 1 component as only daily analyzes are needed. However, modern data assimilation systems that include the stratosphere often have 4 times a day output and can be used to examine the higher frequency wave 2 component of the 4-day wave. This paper presents results of the 4-day wave seen in the temperature and ozone fields produced by a global data assimilation system during a time when the wave 2 component was dominate.

The 4-day wave has been described by Venne and Stanford (1979, 1982), Prata (1984), Lait and Stanford (1988), Randel and Lait (1991), Manney (1991), Lawrence et al. (1995), and Lawrence and Randel (1996). More references can be found in Allen et al. (1997). Most of these studies examined satellite radiances, though Manney (1991) used daily analyzes from the NCEP (National Center for Environmental Prediction) data assimilation system. The wave originates near the stratopause at the level of the stratospheric jet maximum where the latitudinal mean zonal wind shears tend to be

largest. The wave is believed to be a result of barotropic and baroclinic instability depending on the particular zonal mean wind configuration.

The linear barotropic instability problem at the stratopause was first investigated by Hartmann (1983) for idealized latitudinal zonal wind profiles. Hartmann (1983) found that instabilities could occur on both the poleward and equatorward side of jets corresponding to negative zonal mean potential vorticity gradients on both sides of the jet. The rotational phase speeds of the waves were nearly equal to the mean zonal wind speed where $\bar{q}_y$ (the zonal mean potential vorticity gradient) changed sign. This gives shorter rotational periods on the poleward side of the jet ($\sim$4 days) and longer rotational periods on the equatorward side of the jet ($\sim$15 days) because of the change in length of latitude circles around the globe, even though the phase speeds could be similar on both sides of the jet. Using a quasi-geostropic model Hartmann (1983) also found that baroclinic effects tended to stabilize and reduce growth rates by confining the vertical extent of the strong latitudinal wind shear region. Another barotropic model study (Manney et al. 1988) showed that wave 2 became the most unstable mode, rather than wave 1, as the jet became more sharply peaked and that the waves became more dispersive (that is, the rotational period had more variation for different wave numbers) as the jet moved equatorward.

Manney and Randel (1993) used a linear quasigeostropic model to examine unsta-

ble modes in climatological zonal mean winds, including both barotropic and baroclinic effects. They showed that both effects were necessary for realistic growth rates to occur in the zonal mean winds they studied. These results agreed with observational studies (Randel and Lait 1991) that showed strong vertical Eliassen-Palm (EP) fluxes in some analysis of 4-day wave observations. More recent work by Allen et al. (1997) highlighted the general structure of the 4-day wave in terms of the temperatures, winds, and heights associated with a potential vorticity (pv) anomaly.

Stratospheric tracers can respond to the 4-day wave if they have mean gradients in the wave region. Using observations from UARS (Upper Atmosphere Research Satellite) Allen et al. (1997) showed the 4-day signal in ozone while Manney et al. (1998) showed the 4-day signal in water vapor and methane. Both studies modeled the tracers differently. Allen et al. (1997) calculated the linear ozone response to the observed temperature and geostropic meridional wind signal coupled with simple photochemistry. Manney et al. (1998) used an isentropic transport model to examine how tracers were incorporated into the wave region and distributed with latitude. Both studies showed that the 4-day wave, when active, can explain a large amount of the tracer variability near the polar stratopause.

This paper reports on the higher frequency, wave 2 component of the 4-day wave using 4 times a day output from a data assimilation system that includes ozone as well

as the standard mass and wind fields. Following a brief description of the assimilation products and analysis methods (section **2.**) the assimilation based 4 day wave diagnostics are presented (section **3.**). In addition to the DAO ozone assimilation the 4 day wave can be seen in POAM observations (section **4.**).

2. Analysis

This study uses assimilation products from the Data Assimilation Office (DAO) at Goddard Space Flight Center (GSFC). Output is taken from a development system (fvDAS: finite volume Data Assimilation System) that was run for the year 1998. This system is based on the new fvGCM (finite volume General Circulation Model) coupled with the PSAS (Physical space Statistical Analysis System) analysis system (Cohn et al. 1998). PSAS is used in the current DAO operation system. The fvGCM should be part of the operational system in 2002. The fvGCM has the advantage in the stratosphere of being less noisy than the current production system model. As in the current DAO production system, the top analysis level is 0.4 hPa with the actually model top at 0.01 hPa making this a good system for stratopause studies. Output from the fvDAS includes zonal and meridional winds, temperature, and heights on 36 pressure levels from 1000–0.2 hPa at 2.5 by 2° longitude by latitude horizontal resolution. These output fields were saved

every 6 hours.

In addition to the regular assimilation system, an off-line ozone assimilation has been run for the same time period (1998) using the fvDAS winds and temperatures as input (Stajner et al. 2001). The assimilation uses ozone observations from SBUV (Solar Backscatter Ultra-Violet) for profile information and from TOMS (Total Ozone Measuring Spectrometer) for a total column constraint. The ozone fields are available on the same grid and at the same times as the fvDAS assimilation describe above.

Standard Fourier transform packages are used on two dimensional longitude by time arrays to extract the eastward propagating wave components of interest. The Fourier analysis was done monthly (120–124 points in time). The westward propagating modes consist mainly of solar tidal periods and are not shown here. Though some higher wavenumber components also show the 4-day wave, only the dominant wave 1 and wave 2 components are presented here. EP fluxes and associated heat and momentum fluxes were calculated for a given wavenumber and frequency from the zonal wind, meridional wind, and temperature Fourier coefficients along with the zonal and monthly averaged zonal winds and temperatures. The EP flux formulas were evaluated in spherical, log-pressure coordinates (see Andrews et al. 1987, equations 3.5.3a and b, page 128).

3. Results

The 4-day wave is easily seen in the assimilation products. Fig. 1 shows longitude time sections for temperature and ozone at 70°S and 2 hPa for July 1998. Both fields show wave 2 features propagating eastward with periods of about 2 days. The peak to peak amplitude is on the order of 10 K for temperature and 1 ppmv for ozone. A comparison with independent POAM ozone observations will be given later.

Fig. 2 gives a mid-July, 2 hPa synoptic view of the south pole where the wave 2 structure can be easily seen. The temperature field (fig. 2a) shows two warm regions with a cold, elongated region in between, over the pole. Both of these warm regions are also seen in the UKMO (United Kingdom Meteorological Office) stratospheric assimilation (not shown) so the warm regions are not likely to be a DAO system artifact. However, there are differences in temperatures between the two analyzes that reflect the difficulties still associated with temperature analyzes near the stratopause. The Ertel potential vorticity (pv) field (fig. 2b) shows a strong gradient associated with the main polar vortex and a weaker, inner vortex, associated with the wave 2 feature. Ozone (fig. 2c) also shows an elongated wave 2 low ozone region near the pole. The phase of the ozone disturbance is somewhat east of the temperature and pv waves. In addition, the zonal wind component (fig. 2d) shows a wave 2 shaped region of weak winds over

the pole. The zonal wind is of interest because its meridional derivative can help create the negative regions of potential vorticity gradient, q_y, needed for instability of the zonal flow. Negative regions of quasi-geostropic potential vorticity gradient are shaded in fig. 2d. The three negative regions associated with the inner vortex will change with time as the fast inner vortex interacts with the slower changing main vortex. Though this paper focuses on the waves interacting with a zonally averages basic state, the complicated negative q_y pattern, with its lack of zonal symmetry, should be kept in mind. In addition to wave 2, the patterns in fig. 2 show a wave 1 component as well, in that the disturbance is centered somewhat off the pole, however, the wave 2 feature stands out clearly at this time.

A representative 6 month time series (April–September 1998) of temperature and ozone at a point at 70°S and 2 hPa (fig. 3) shows 2–4 day fluctuations throughout the time period. The temperature and ozone oscillations increase in amplitude in July 1998, though the ozone shows larger amplitudes than temperature in May and June. There is some visual evidence here (and it has been verified by spectral analysis) that the period of the oscillations is higher in July than in August. This corresponds to the dominance of wave 2 over wave 1 in July.

Fig. 4 shows the zonal average temperature and ozone at 2 hPa as a function of time and latitude. While the ozone gradients increase somewhat with time, the temperature

structure changes dramatically in July 1998, with a relatively warm region forming at 60-70°S and increased meridional temperature gradients poleward of 70°S. As will be shown, this warm region is where the wave 2 component of the 4-day wave is found.

Results for the July spectral analysis of temperature and ozone are shown for eastward propagating wave 1 and wave 2. Fig. 5 shows the frequency spectrum as a function of pressure at 70°S. Also plotted is the critical line, derived from the zonal mean zonal wind, for each frequency and wavenumber. Note that most wave activity is constrained by the critical line indicating that the waves are regressing with respect to the zonal mean winds as expected for Rossby waves. The wave 1 temperature spectra (fig. 5a) are large for the stationary and slowly propagating waves, however, the amplitudes are relatively weak and poorly defined near the 4-day wave frequency ($0.25\ \mathrm{day}^{-1}$). The wave 1 ozone spectra (fig. 5b) shows a stationary wave peak at 2 hPa and a weak ozone peak at a fairly high period ($0.4\ \mathrm{day}^{-1}$) right at the critical level. The wave 2 temperature spectra (fig. 5c) shows a large, vertically coherent peak, at about $0.6\ \mathrm{day}^{-1}$. This is the wave 2 structure of interest. The period is about 1.7 days. The spectral peak has a maximum between 1–2 hPa and extends from the top of the domain down to the critical level. The wave 2 ozone spectra (fig. 5d) shows a similar $0.6\ \mathrm{day}^{-1}$ peak, though much more localized in the vertical than the wave 2 temperature peak. It also tends to show a weak peak at higher frequencies near the critical level, similar to

the wave 1 ozone spectra.

The same frequencies as a function of latitude, at 2 hPa, are shown in fig. 6. Once again the waves are generally constrained by the critical line to be propagating more slowly than the zonal mean flow. An exception seen here is on the equator where the peaks in the temperature spectra are likely to be Kelvin waves. The wave 1 temperature spectra (fig. 6a) shows the largest amplitudes at low frequencies (periods greater than 10 days). Poleward of 70°S there is a weak peak right at the 0.25 day^{-1} frequency. The wave 1 ozone spectra (fig. 6b) shows the low frequency waves along with high frequency peaks poleward of 70°S. As in fig. 5, the ozone tends to show peaks at the critical level and peaks beyond the critical level. The wave 2 temperature spectra (fig. 6c) shows low frequency waves equatorward of 60°S and the high frequency peak, as before, at 0.6 day^{-1}. The wave 2 ozone spectra (fig. 6d) also show the 0.6 day^{-1} peak, along with peaks at higher frequency near the critical levels. The tendency seen here for the ozone to peak at the critical level probably represents advection of ozone features by the zonal mean wind. Fig. 6 shows that the high frequency wave is larger and more well defined in wave 2 than wave 1 during July 1998 in agreement with fig. 5.

As pointed out by Allen et al. (1997) and others the 4-day wave temperature structure is expected to be a vertical dipole about a height (or pv) perturbation. The two lobes of the temperature dipole will be out of phase with each other so that high pertur-

bation heights will have warm air below and cold air above, consistent with hydrostatic balance. In this study, only the lower lobe of the temperature dipole can been seen, as the DAO pressure level output stops above 0.2 hPa. However, the height and pv waves can be examined above the lower temperature lobe.

Figure 7 shows the wave 1 and wave 2 pv and height spectra for July 1998 at 0.4 hPa as a function of latitude. The pv and height spectra are similar. The wave 1 spectra (figs. 7a and b) show the largest peaks for the low frequency waves with smaller peaks poleward of 70°S at 0.25 day^{-1} and higher frequencies. The wave 2 spectra (figs. 7c and d) show some low frequency waves equatorward of 60°S and a well defined high frequency peak at 0.6 day^{-1}. This wave 2 peak occurs near the intersection of the critical line and the latitude where $\bar{q}_y = 0$. This agrees with expectations from the linear theory of barotropically growing waves. Because of the double peaked jet at these altitudes, the wave 2 frequencies from 0.55–0.6 day^{-1} actually have three critical lines (as can be seen in fig. 7), and the two most poleward critical lines are close to the two $\bar{q}_y = 0$ lines that bound the negative $\bar{q}_y$ region between the two jets. Thus, the monthly averaged zonal mean zonal wind in July 1998 provides ample opportunity for the development of wave 2, 0.55–0.6 day^{-1} waves. What is not clear is why wave 2 is singled out for development rather than the corresponding wave 1 frequencies.

The next three plots (figs. 8, 9, and 10) present a series of latitude pressure sections

of the July 1998 wave 2 structure at a single frequency, 0.58 day^{-1} (1.72 day period), that corresponds to the main wave 2 peak seen in the spectra. The critical line for this frequency is repeated on all the plots as a reference line. Note that these plots are more limited in altitude (100–0.2 hPa) and latitude (90–30°S) than previous plots to better focus on the region of interest.

Figure 8a shows the zonal mean zonal wind for the month of July 1998 and its associated negative region of $\bar{q}_y$. The jet tilts strongly equatorward with altitude with a weak poleward secondary maximum at the uppermost levels. In between the two jets is the negative $\bar{q}_y$ region. The critical line for the 0.58 day^{-1} wave and the $\bar{q}_y = 0$ line coincide at upper levels, in the region between the two jets. The reference level at 0.4 hPa shows how there can be three critical levels at a given altitude as seen in fig. 7 Figure 8b shows the zonal mean July 1998 temperatures. The dashed line shows where the horizontal temperature gradient is zero. A region of reversed temperature gradient (warm air toward the pole) extends down from the mesosphere into the stratosphere.

Figure 8c shows the wave 2 temperature amplitude and phase. As mentioned above, only the lower lobe of the temperature structure is seen at these altitudes, though the phase is changing rapidly with height at the top level, as expected, and there is some hint of an increase in amplitude beginning at 0.2 hPa. The temperature wave maximum (about 2.5 K) is occurring right where the mean temperature gradients are reversed

(fig. 8b). The ozone amplitude maximum (fig. 8d) is poleward and lower than the temperature amplitude. The ozone amplitude (maximum about 0.2 ppmv) is more confined in the vertical than the temperature amplitude and the ozone phase emphasizes the change in phase with latitude.

Figure 9a shows the wave 2 height field for July 1998. The maximum height amplitude (about 80 m) is near the critical line. The phase structure will be discussed below along with the EP (Eliassen-Palm) flux. Using output from a data assimilation system allows for examination of quantities not normally seen, such as vertical velocity (fig. 9b). The vertical velocity perturbation is seen to peak (about 0.8 x10^{-2} m s^{-1}) in the negative $\bar{q}_y$ region at the highest levels examined.

Figure 9c superimposes the ozone amplitude on top of a plot of the horizontal gradient of the zonal mean ozone. The ozone wave amplitude corresponds to where the height wave amplitude (fig. 9a) overlaps the horizontal ozone gradient, implying that horizontal advection by the wave is mainly responsible for the ozone wave signal, in agreement with the findings of Manney et al. (1998).

Figure 9d shows that temperature is not the only quantity with a dipole structure. The zonal mean wind perturbation shows a strong dipole structure in latitude associated with the height perturbation. A phase switch occurs between the two lobes. This structure is expected from geostropic balance with the perturbation height field. The

most equatorward lobe peaks at 50°S.

Figure 10a plots the EP flux divergence and the EP flux vectors calculated from the assimilated winds and temperatures for July 1998 wave 2 height field. The divergence is centered at about 1 hPa and 58°S with extensions up into the negative $\bar{q}_y$ region and across over a broad latitude range (70–50°S) at 2 hPa. The EP flux vectors point into three convergence regions: equatorward (and above), poleward (and above) and below the divergence region. Linear instability theory predicts growing waves to consist of a dipole of EP flux divergence and convergence with the EP flux vector pointing from divergence to convergence (see Hartmann (1983) for a discussion of the barotropic problem and Manney and Randel (1993) for baroclinic examples). The July 1998 wave 2 shows a more complex case than what is usually modeled. The poleward and equatorward EP flux vectors shows that both poleward and equatorward momentum fluxes are associated with the wave. This helps explain the height field phase variation shown in fig. 9a at upper levels where the meridional phase gradient changes sign. Downward EP flux vectors have been seen by Randel and Lait (1991) and Allen et al. (1997) and in the linear instability model of Manney and Randel (1993). These downward EP flux vectors are not surprising in a middle atmosphere instability event, however, they are opposite the usually upward direction associated with planetary waves coming from the troposphere. The net EP flux will still be upward, of course, as the forced upward

planetary fluxes are much larger than the fluxes associated with the local instability. These downward EP flux vectors continue to below 10 hPa where the stop near the lower part of the critical level.

Figure 10b shows the same fields as in fig. 10a, calculated using only the assimilated height field amplitude and phase shown in fig. 9a, using the quasi-geostropic approximation. Though the magnitudes are larger, the quasi-geostropic approximation shows remarkable agreement with the full calculation. This lends support to studies based only on satellite derived heights.

Figure 10c plots the heat flux based mass stream function (meridional heat flux divided by the mean stability) associated with the 0.58 day^{-1} wave 2. The circulation is equatorward at 2 hPa, opposite to the poleward motion usually associated with the upward propagating planetary waves. The total circulation will be dominated by the upward propagating planetary waves however, the higher frequency wave signal can be seen as a perturbation in the over all downward poleward motion (not shown).

The EP flux divergence is re-plotted (fig. 10d) scaled by density to reflect the mean wind tendency. Most of the tendency occurs at the lowest density level shown, with the EP flux divergence acting to increase the wind in the region between the two jets and with the EP-flux convergence acting to decrease the jet winds, especially the poleward jet. The maximum de-acceleration shown is about 4 m s^{-1} day^{-1}.

The time behavior during July 1998 is examined by first putting the assimilation fields through a simple band pass filter that truncates the fft so that only eastward propagating wave 2 frequencies between 0.4–1.0 day^{-1} are retained. Figure 11a shows the EP flux divergence at 2 hPa as a function of latitude and time based on the filtered assimilation products. The EP flux divergence shows how the wave forcing changes over the course of the month. The peak of the EP flux divergence varies from about 55°S early in the month to 60–70°S later in the month. The largest values of EP flux divergence start on 13 July 1998 and consist of six events (13, 16, 18, 22, 25, and 28 July). Figure 11b shows the time evolution of the zonal mean zonal wind along with the 0.58 day^{-1} critical level and the negative $\bar{q}_y$ regions, all at 2 hPa. The three later EP flux divergence peaks (22, 25, and 28 July) are seen to occur about a half a day after the center of corresponding negative $\bar{q}_y$ regions. There is also some overlap between the EP flux divergence on 9 July and a negative $\bar{q}_y$ region.

Figure 12 shows the same fields as fig. 11 at 0.4 hPa. The zonal mean zonal wind (fig. 12b) shows the double jet structure at these altitudes with a persistent region of negative $\bar{q}_y$ located between the two jets. Unlike the nearly constant single critical line at 2 hPa, at 0.4 hPa there are often times when the 0.58 day^{-1} critical line is found at three latitudes. Note how the 0.58 day^{-1} critical line mirrors the poleward most $\bar{q}_y = 0$ line during most of the time shown and tracks closely the middle critical line about half

of the time shown. The EP flux divergence at 0.4 hPa is mainly in the negative $\bar{q}_y$ region with EP flux convergence outside the negative $\bar{q}_y$ region as expected from linear stability for growing waves. This relation is especially apparent on 14 July.

Figure 13 shows the EP flux divergence and the zonal mean zonal wind at 4 times: 7 Jul 6 UTC, 13 Jul 18 UTC, 18 Jul 0 UTC, and 22 Jul 6 UTC. Because these fields are not time averages and contain a range of frequencies the magnitude of the EP flux vectors and their divergences are larger than in the monthly averaged, single frequency plots shown in fig. 10 and the vectors and contours have been re-scaled for these plots. Early in the month (fig. 13a) the EP flux divergence is relatively weak and located at a relatively low latitude (55°S). There are two EP flux convergence regions both poleward and equatorward of the divergence with EP flux vectors pointing from the divergence region into the convergence regions. These vectors correspond to both equatorward and poleward momentum fluxes at this time. This pattern of EP flux divergence will tend to accelerate the winds between the split jet (fig. 13b) and de-accelerate both jets. The EP flux divergence at this time is somewhat correlated with the negative $\bar{q}_y$ region located between the split jet

By 13 July, the EP flux divergence (fig. 13c) is much stronger and peaks farther poleward (65°S). While the EP flux divergence peaks below the negative $\bar{q}_y$ region, there is still an EP flux divergence region above 1 hPa that is well correlated with

the negative $\bar{q}_y$ region. There are two EP flux convergence regions at this time: one above and poleward of the main divergence peak, and one below the EP flux divergence region. The EP flux vectors are mainly poleward at this time (equatorward momentum fluxes) except down near 10 hPa where the EP flux vectors head toward the critical level (fig. 13d).

An even more poleward EP flux divergence peak is found on 18 July (fig. 13e) and it is clearly associated with a high latitude negative $\bar{q}_y$ region. The poleward jet is very weak at this time (fig. 13f) and most of the EP flux vectors equatorward of 70°S are equatorward (poleward momentum flux). The EP flux convergence region completely encircles the divergence region with especially strong convergence above and below the divergence region.

Just 4 days later (about one rotational period) the EP flux divergence peak (fig. 13g) is more equatorward (58°S) and there are large regions of both poleward and equatorward EP flux vectors. The EP flux divergence is well correlated with a negative $\bar{q}_y$ region and the double jet structure has returned (fig. 13h). The EP flux convergence region wraps almost completely around the divergence region.

4. POAM

This section presents some POAM (Polar Ozone and Aerosol Measurement) observations (Lucke et al. 1999) as an independent validation of the 4-day wave as seen in the DAO ozone assimilation. During July 1998 the POAM ozone observations were all between about 65–70°S so will be treated as being at a constant latitude. There are ∼14 ozone profiles taken each day. This does not give much resolution for a longitude time plot, nevertheless, fig. 14 shows one attempt to interpolate the longitude time POAM observations at 2 hPa to a regular grid suitable for contouring the high frequency waves. Comparing with fig. 1b, the POAM observations show a similar time mean wave 1 structure and similarly propagating wave 2 features. The amplitude of the wave 2 signal in the POAM observations is about half that of the DAO (the contour interval is doubled in fig. 14) and there is an offset to lower values of ozone in the POAM observations.

More quantitative evidence of the high frequency wave in the POAM observations is shown in fig. 15 using an analysis method similar to that of Prata (1984). Here the POAM observations at each level are taken as a time series for the month. Spectral analysis of the time series confirms what can easily be seen as the largest signal in the time series: an oscillation near 3 hPa with a frequency of 2.58 days^{-1}. A stationary

wave 2 would have a peak of 2 days^{-1} and an eastward propagating wave 2 would have 2 days^{-1} added to its frequency, in this case 0.58 days^{-1}, exactly the peak seen in the DAO ozone assimilation and temperature (fig. 5). Of course, this interpretation of the POAM observations is not unique. The peak at 2.58 days^{-1} could be a very rapidly moving eastward wave 1 or a westward propagating wave 3. However, the wave 2 interpretation seems most likely in this case, given the DAO assimilation results. Only a portion of the POAM spectrum is shown in fig. 15, however, the 2.58 day^{-1} frequency peak is by far the largest spectral peak. The magnitude of the 2.58 day^{-1} peak is about the same as that found in the DAO ozone spectra, though at a lower altitude.

Figure 15 also shows the stationary wave 1 signal (seen in fig. 14) at 1 day^{-1} and a very small peak at 1.4 day^{-1} that can be interpreted as the small wave 1 ozone peak seen in fig. 5b at 0.4 day^{-1}. As pointed out in the discussion of fig. 5b, this peak is right at the mean wind speed, though the POAM spectral peak is at a slightly lower altitude.

5. Discussion

The assimilation products shown here clearly display high frequency waves during the southern hemisphere winter. Issues to be discussed concern the quality of the assimila-

tion products for high frequency wave studies, the ability of linear instability theory to explain the results, and the advective peaks seen in the ozone spectra.

a. Quality

The meteorological data going into the fvDAS at these levels (2 hPa) are mainly satellite radiance measurements. That these observations contain the 4-day wave is not surprising given that the early work in studying the 4-day wave (Venne and Stanford 1979, 1982; Prata 1984) was based directly on satellite radiances. The fvDAS used a direct assimilation of satellite radiances and should reflect any waves in the radiances, however a good representation of the waves is needed in the GCM as well. The ability of the fvGCM to realistically represent these wave has not been studied.

The top level of the analysis my be too low to completely characterize the waves. As mentioned in the introduction, the top analysis level is 0.4 hPa with the highest pressure level output being slightly above at 0.2 hPa. The negative $\bar{q}_y$ region and the wave 2 critical level extends above this altitude. It would be more satisfying if the entire unstable and high zonal wind speed regions were captured. However, the fvGCM does extend upward to 0.01 hPa so the whole region of instability may be contained by the fvDAS.

The ozone data assimilation system was being run without chemistry at this time, relying on observations to correct it for chemistry. This may lead to some biases in the mean values and wave amplitudes in the ozone assimilation, however, the basic patterns should follow the advection by the fvGCM combined with the ozone observations. Past studies have shown the 4-day wave signal in ozone (Allen et al. 1997) and other tracer gases (Manney et al. 1998). Here, the 4-day wave signal was shown to be strongly supported by POAM observations as well.

The use of band passed filtered fields was used here because the 2-day wave signal was well defined and persistent throughout July 1998. Generally the band passed filtered fields closely followed the full wave pattern (by comparison of corresponding maps, not shown), however, there were some specific times (mainly at the end of the month) when the band passed filtered temperatures did not closely resemble the warm temperature regions. These times show larger wave 1 and wave 3 components involved. More spectral components need to be considered or a non Fourier approach taken for detailed study at these times.

The key to this study was to have the fvDAS products available every 6 hours. This time resolution allows for the detailed study of these fast propagating as fast changing waves.

b. Instability theory

In linear instability theory the negative $\bar{q}_y$ region is correlated with the EP flux divergence region. Hartmann (1983) found his barotropic model to be exactly correlated. Results shown in Manney and Randel (1993) suggest EP flux divergence and negative $\bar{q}_y$ in their baroclinic model is very closely correlated as well. Our EP flux divergence plots are not so well correlated with negative $\bar{q}_y$ regions. Throughout the month of July 1998, the EP flux divergences are closely associated with a negative $\bar{q}_y$ region, however, the negative $\bar{q}_y$ regions seem to disappear quickly once the EP flux divergence region appears. The negative $\bar{q}_y$ region is never completely eliminated, however, but tends to shift to a different latitude or height.

Some of the wave structure seems to show wave propagation away from the source region toward convergence at the critical level. This can be seen in fig. 10a where the EP flux vectors converge on the critical line at about 20 hPa. In contrast the linear instability EP flux vectors shown in Manney and Randel (1993) are only large close to the negative $\bar{q}_y$ region.

Fig. 2d shows how zonally asymmetric the negative potential vorticity regions can be. This suggests that formulating the problem as waves growing on a zonal mean unstable state may only be a first step in understanding the origin of the waves. All of

the EP flux divergence regions seen in the zonal average sense overlap with negative potential vorticity regions at some longitude (not shown). Additional consideration of wave-wave interactions (Manney et al. 1989) or a more three dimensional approach may be needed.

Overall, our study supports linear instability studies with potential vorticity instability for the origin of the waves. The waves (where $\bar{q}_y$ is positive) propagate more slowly then the mean wind in agreement with Rossby wave theory. In addition the waves vertical scale decreases as the waves approach the critical level below as seen in fig. 9a where the phase of the height field begins to change rapidly, also in agreement with linear Rossby wave theory. The frequency of the wave is determined by the near coincidence of the $\bar{q}_y = 0$ line and a constant zonal mean zonal wind line (critical line) in the region between the double jet.

c. Advective peak

While the temperature spectra peaks at speeds slower than the zonal mean zonal wind, the ozone spectra shows a tendency for additional peaks at (and faster than) the zonal mean zonal wind speed (fig. 6). This may imply that temperature is more dynamically controlled than ozone. Chemistry or diabatic processes may act to create ozone gra-

dients along pv contours allowing ozone to have a passive advection signal. While no signals like this were seen in Manney et al. (1998) a large fast moving ozone peak was seen in the spectra results presented in Allen et al. (1997). The results here should be interpreted with some caution as these advective peaks were not identified before the spectral analysis and the relation between the spectra of advected tracers to the zonal mean zonal wind speed has not been investigated here.

Past studies of the 4-day wave have sometimes commented on the advective like motion of the warm temperature regions. However, our results suggest that the temperature perturbations are generally moving more slowly than the mean wind. In addition the ozone results serve as a reminder that advection is more likely to produce filaments, rather than well-defined isolated temperature regions. This can be seen to some extent in fig. 2, where the temperature map has less filament structure than the ozone map.

6. Conclusion

This paper has focused on a month when the wave 2 component of the 4-day wave was well defined and persistent. The availability of 4 times daily output from the fvDAS has allowed the first detailed look at this fast moving wave feature. In addition, a companion ozone assimilation allowed identification of the high frequency wave in the

ozone field.

This wave 2 component (1.7 day period) is generally consistent with past observational studies and linear instability models. The EP flux divergence is closely associated with negative $\bar{q}_y$ regions with the wave amplitude mainly confined by the critical line.

The wave 2 also shows a large amplitude in the DAO ozone assimilation, about 0.5 ppmv or 15% of the total ozone at 2 hPa. This ozone signal is supported by independent POAM observations. POAM shows a spectral peak consistent with the assimilation. The amplitude of the signal in POAM is about half the amplitude of the assimilation at 2 hPa but the POAM signal peaks at a slightly lower altitude (3 hPa) and the amplitude there agrees with the DAO ozone assimilation.

In addition to the 4-day wave peaks, the ozone assimilation showed high frequency peaks corresponding to the zonal mean zonal wind speed. These peak may be related to advection of ozone gradients along the pv contours.

While the wave can appear fairly steady over the course of a month, the EP flux divergence pattern can vary significantly over the course of a wave period. This probably indicates that more can be done examining these wave and their development in instantaneous pv maps. This leaves open future studies based on assimilation products to further understand the origin and development of high frequency polar waves.

Acknowledgment Thanks to . . .

References

Allen, D. R., J. L. Stanford, L. S. Elson, E. F. Fishbein, L. Froidevaux, and J. W. Waters: 1997, The 4-day wave as observed from the Upper Atmosphere Research Satelite Microwave Limb Sounder. *J. Atmos. Sci.*, **54**, 420–434.

Andrews, D. G., J. R. Holton, and C. B. Leovy: 1987, *Middle Atmosphere Dynamics*. Academic Press, 489 pp.

Cohn, S. E., A. da Silva, J. Guo, M. Sienkiewicz, and D. Lamich: 1998, Assessing the effects of data selection with the DAO physical-space statistical analysis system. *Mon. Weather. Rev.*, **126**, 2913–2926.

Hartmann, D. L.: 1983, Barotropic instability of the polar night jet stream. *J. Atmos. Sci.*, **40**, 817–835.

Lait, L. R. and J. L. Stanford: 1988, Fast, long-lived features in the polar stratosphere. *J. Atmos. Sci.*, **45**, 3800–3809.

Lawrence, B. N., G. J. Fraser, R. A. Vincent, and A. Philips: 1995, The 4-day wave in the Antarctic mesosphere. *J. Geophys. Res.*, **100**, 18899–18908.

Lawrence, B. N. and W. J. Randel: 1996, Variability in the mesosphere observed by the Nimbus 6 PMR. *J. Geophys. Res.*, **101**, 23475–23489.

Lucke, R. L., D. R. Korwan, R. M. Bevilacqua, J. S. Hornstein, E. P. Shettle, D. T. Chen, M. Daehler, J. D. Lumpe, M. D. Fromm, D. Debrestian, B. Neff, M. Squire, G. König-Langlo, and J. Davies: 1999, The Polar Ozone and Aerosol Measurement (POAM) III instrument and early validation results. *J. Geophys. Res.*, **104**, 18785–18799.

Manney, G. L.: 1991, The stratospheric 4-day wave in NMC data. *J. Atmos. Sci.*, **48**, 1798–1811.

Manney, G. L., T. R. Nathan, and J. L. Stanford: 1988, Barotropic strability of realistic stratospheric jets. *J. Atmos. Sci.*, **45**, 2545–2555.

— 1989, Barotropic instability of basic states with a realistic jet and a wave. *J. Atmos. Sci.*, **46**, 1250–1273.

Manney, G. L., Y. J. Orsolini, H. C. Pumphrey, and A. E. Roche: 1998, The 4-day wave and transport of UARS tracers in the austral polar vortex. *J. Atmos. Sci.*, **55**, 3456–3470.

Manney, G. L. and W. J. Randel: 1993, Instability at the winter stratopause: A mechanism for the 4-day wave. *J. Atmos. Sci.*, **50**, 3928–3938.

Prata, A. J.: 1984, The 4-day wave. *J. Atmos. Sci.*, **41**, 150–155.

Randel, W. J. and L. R. Lait: 1991, Dynamics of the 4-day wave in the Southern Hemisphere polar stratosphere. *J. Atmos. Sci.*, **48**, 2496–2508.

Stajner, I., L. P. Riishojgaard, and R. B. Rood: 2001, The GEOS ozone data assimilation system: Specification of error statistics. *Q. J. R. Met. Soc.*, **127**, 1069–1094.

Venne, D. E. and J. L. Stanford: 1979, Observations of a 4-day temperature wave in the polar winter stratosphere. *J. Atmos. Sci.*, **36**, 2016–2019.

— 1982, An observational study of high-latitude stratospheric planetary waves in winter. *J. Atmos. Sci.*, **39**, 1026–1034.

List of Figures

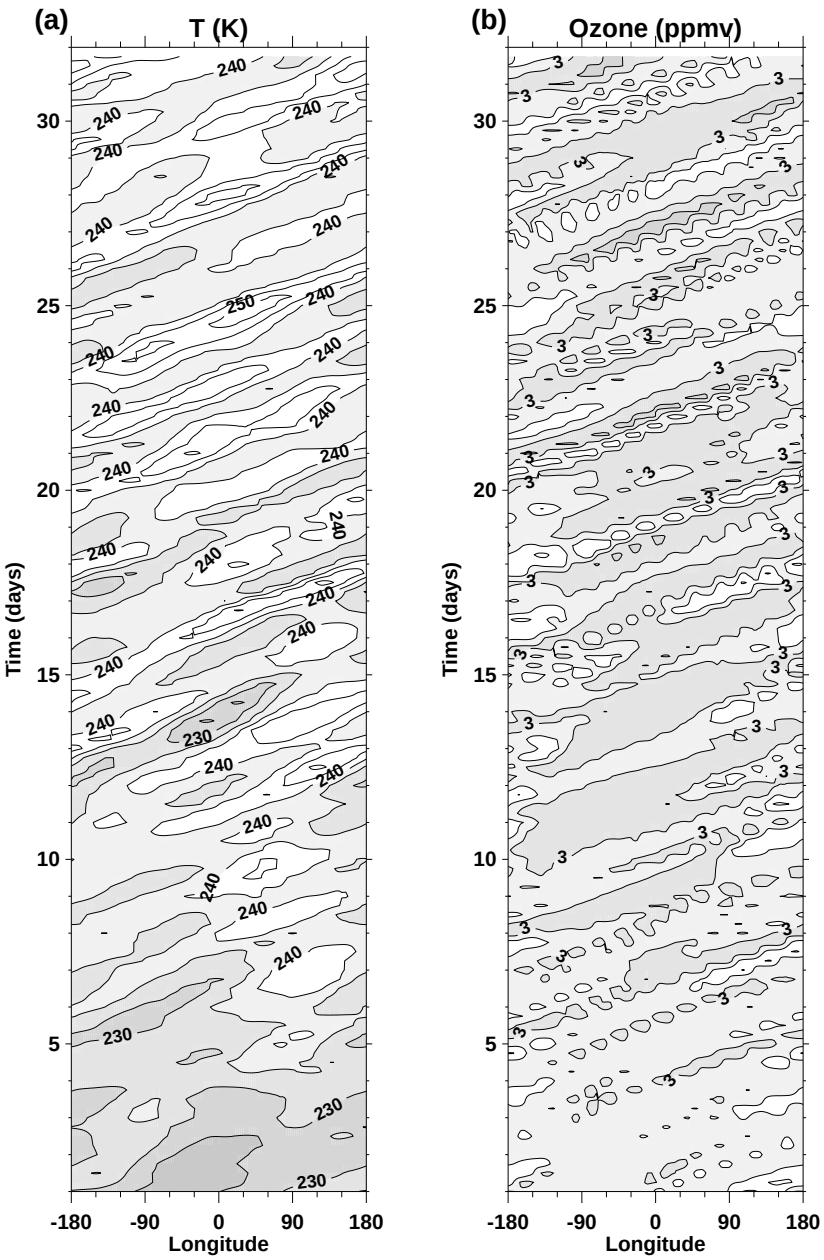

Figure 1: Longitude time plot of (a) temperature (K) and (b) ozone (ppmv) at 70°S and 2 hPa for July 1998. Temperature contour interval is 5 K. Cooler temperatures are shaded. Ozone contour interval is 1 ppmv. Lower ozone values are shaded.

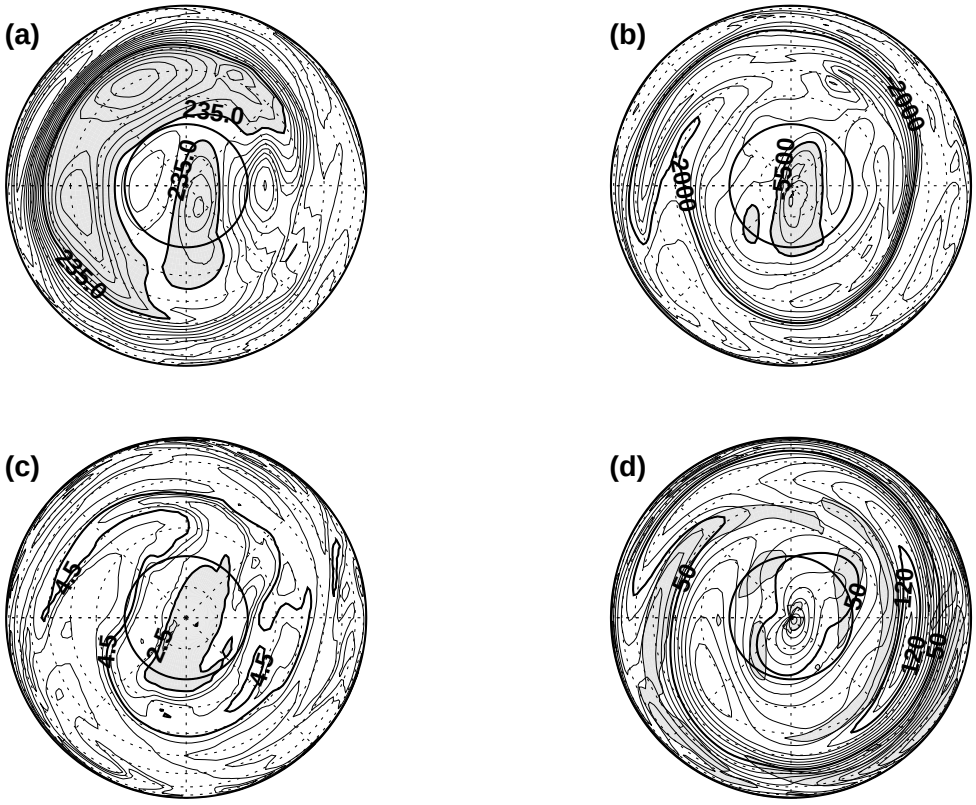

Figure 2: Circulation at 2 hPa on 16 July 12Z: (a) temperature (K), temperatures less than 235 K shaded, contour interval 2.5 K, (b) potential vorticity (pvu, where 1 pvu = 1×10^{-6} K m^2 kg^{-1} s^{-1}) pv less than -5500 pvu shaded, contour interval 500 pvu, (c) ozone (ppmv), ozone less than 2.5 ppmv shaded, contour interval 0.5 ppmv, and (d) zonal wind component (m s^{-1}), q_y less than zero is shaded, contour interval 10 m s^{-1}. Orthographic projection from equator to south pole, 90° east at the bottom of the plots, highlighted latitude at 70° south.

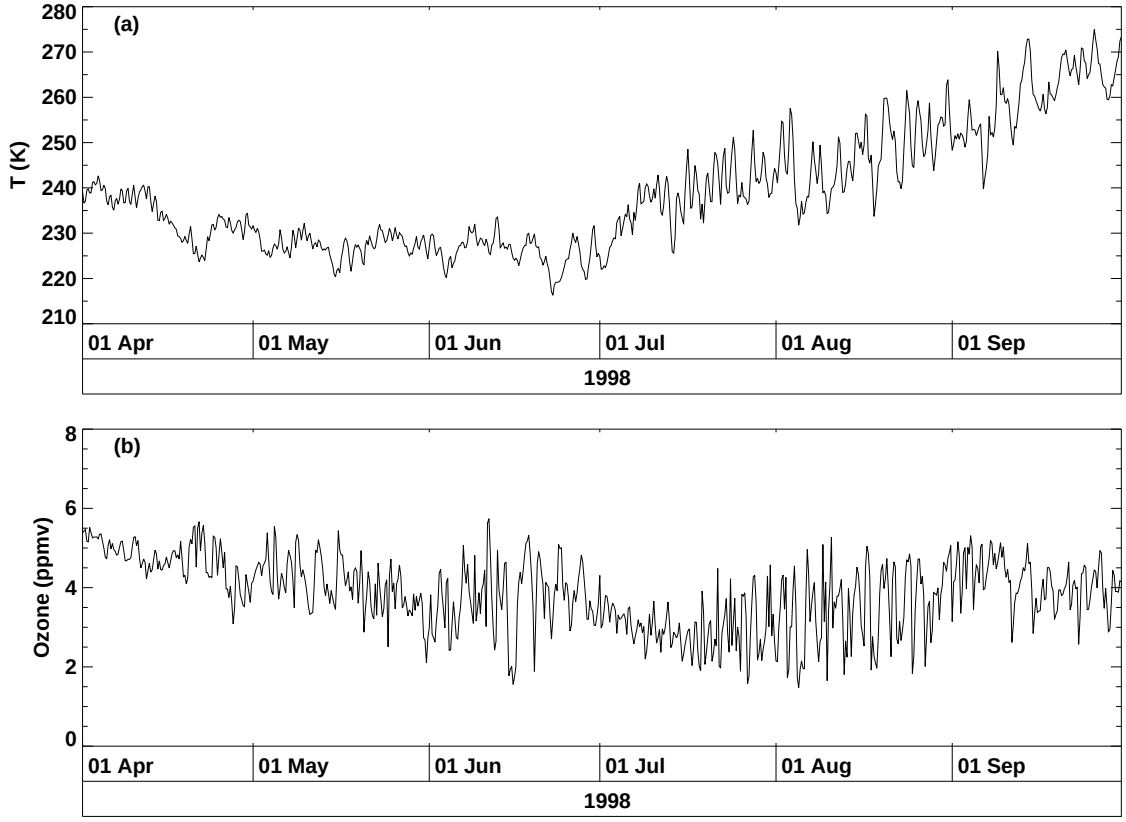

Figure 3: Time series of (a) temperature (K) and (b) ozone (ppmv) at 0° longitude, 70° south latitude. Time resolution is 6 hr. Altitude is 2 hPa.

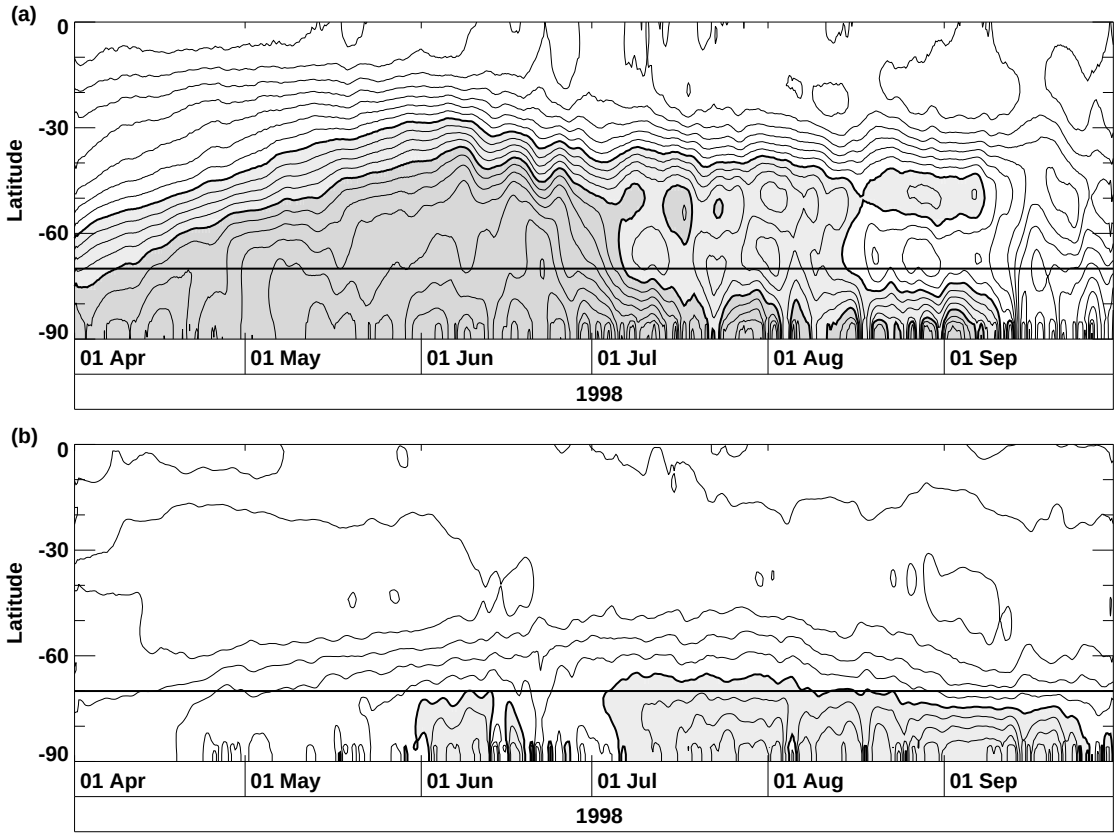

Figure 4: Latitude time contour plot of (a) temperature (K), 5 K contour interval, dark shading: temperatures less than 235 K, light shading: temperatures less than 245 K and (b) ozone (ppmv), 1 ppmv contour interval, shading: ozone less than 3.5 ppmv. Altitude is 2 hPa.

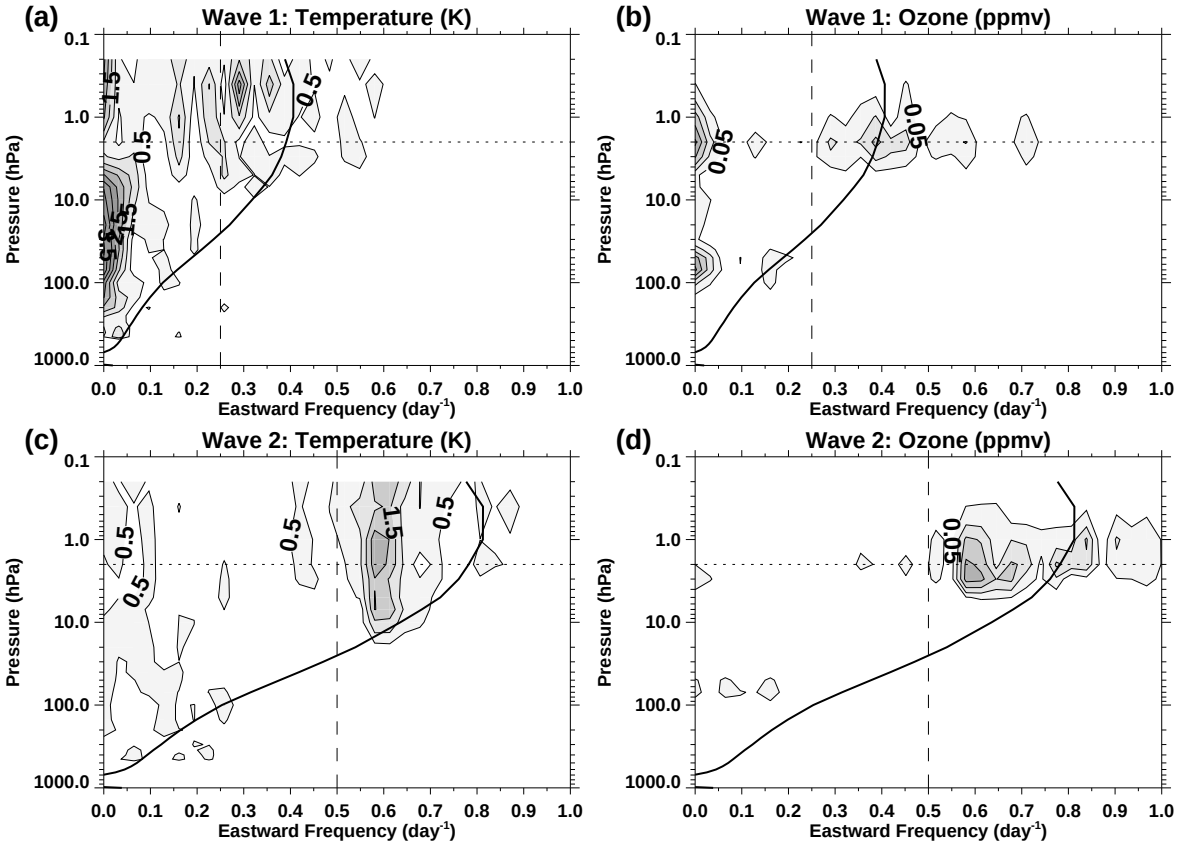

Figure 5: July 1998 wave amplitudes as a function of frequency and pressure at 70°S: (a) wave 1 temperature (K), (b) wave 1 ozone (ppmv), (c) wave 2 temperature (K), and (d) wave 2 ozone (ppmv). Temperature contour interval 0.5 K. Ozone contour interval 0.05 ppmv. The dark line plots the critical level at 70°S. The vertical dashed lines highlight the 4 day (for wave 1) and 2 day (for wave 2) frequencies. The horizontal dotted line is at 2 hPa. Values below 500 hPa are not shown. Larger amplitudes are shaded.

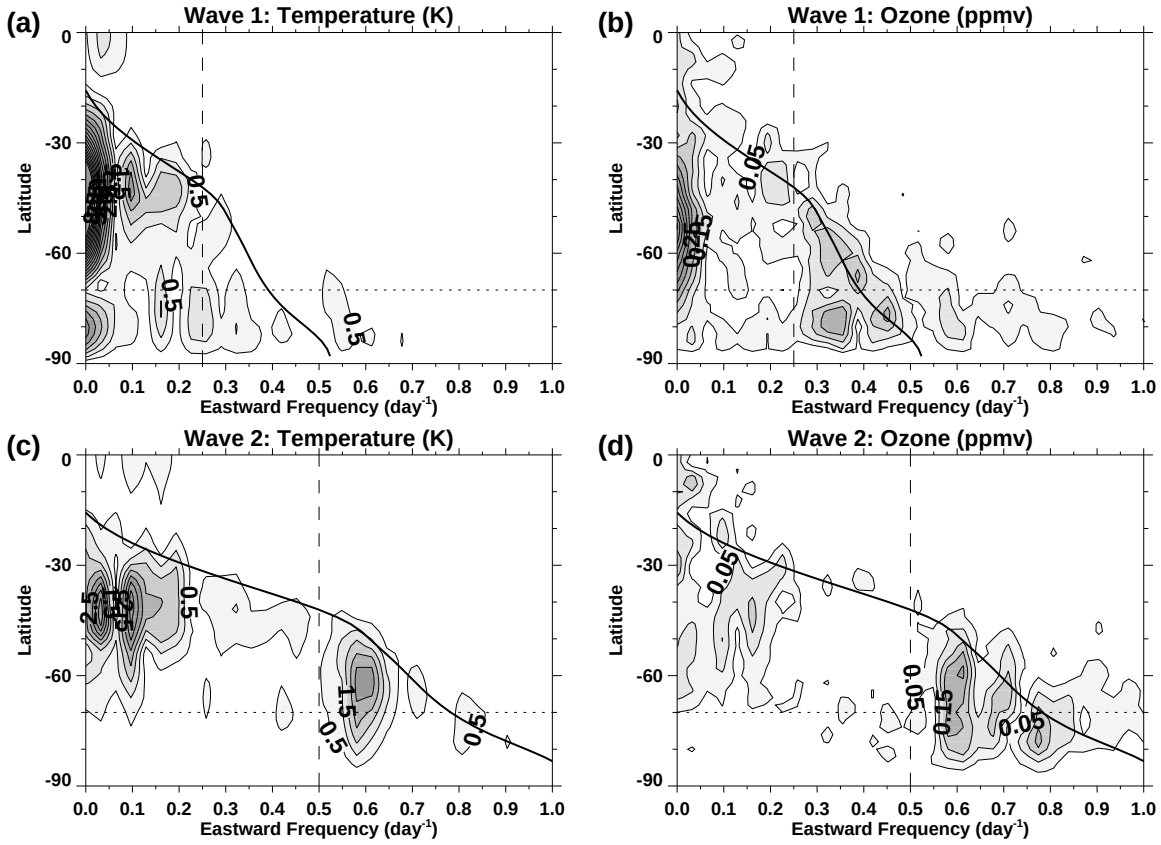

Figure 6: July 1998 wave amplitudes as a function of frequency and latitude at 2 hPa: (a) wave 1 temperature (K), (b) wave 1 ozone (ppmv), (c) wave 2 temperature (K), and (d) wave 2 ozone (ppmv). Temperature contour interval 0.5 K. Ozone contour interval 0.05 ppmv. The dark line plots the critical level at 2 hPa. The vertical dashed lines highlight the 4 day (for wave 1) and 2 day (for wave 2) frequencies. The horizontal dotted line is at 70°S. Larger amplitudes are shaded.

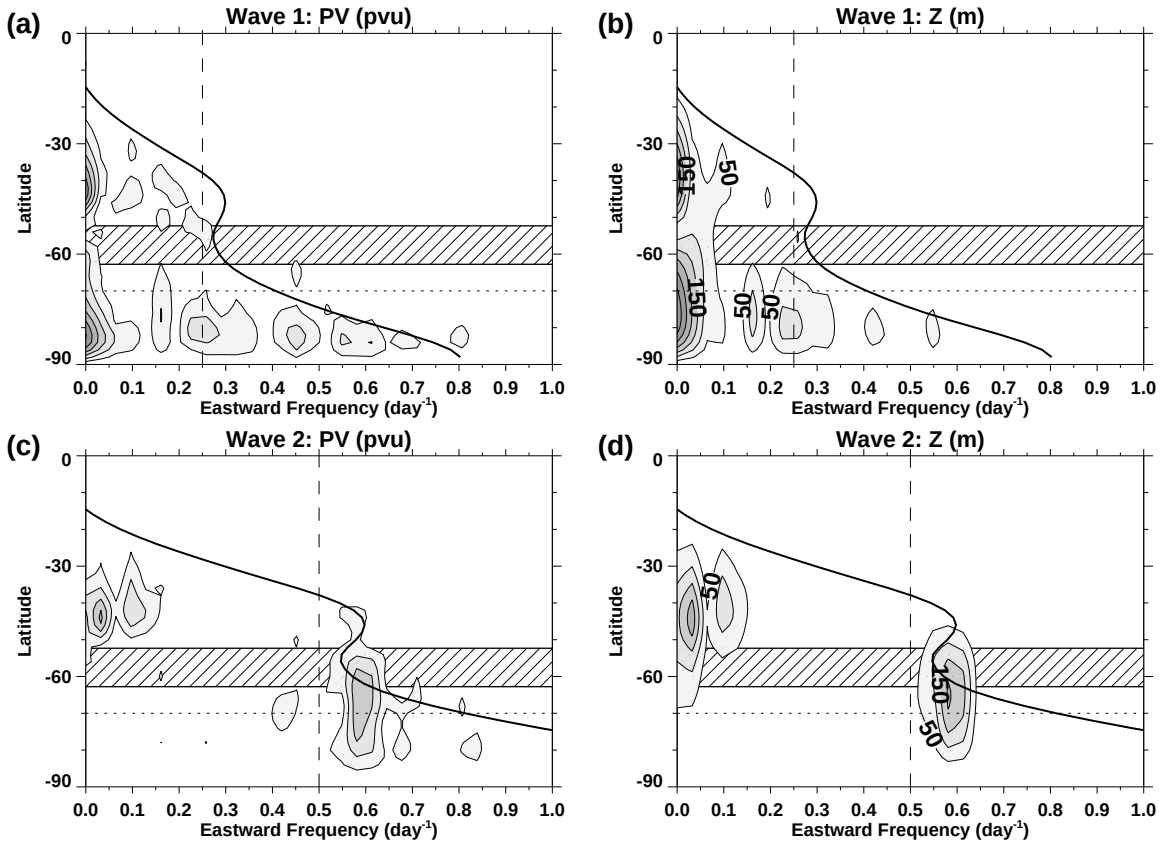

Figure 7: July 1998 wave amplitudes as a function of frequency and latitude at 0.4 hPa: (a) wave 1 potential vorticity (pvu), (b) wave 1 geopotential heights (m), (c) wave 2 potential vorticity (pvu), and (d) wave 2 geopotential heights (m). Potential vorticity contour interval 1000 pvu. Geopotential height contour interval 50 m. The dark line plots the critical level at 0.4 hPa. The diagonally striped region denotes latitudes where $\bar{q}_y$ is negative. The vertical dashed lines highlight the 4 day (for wave 1) and 2 day (for wave 2) frequencies. The horizontal dotted line is at 70°S. Larger amplitudes are shaded.

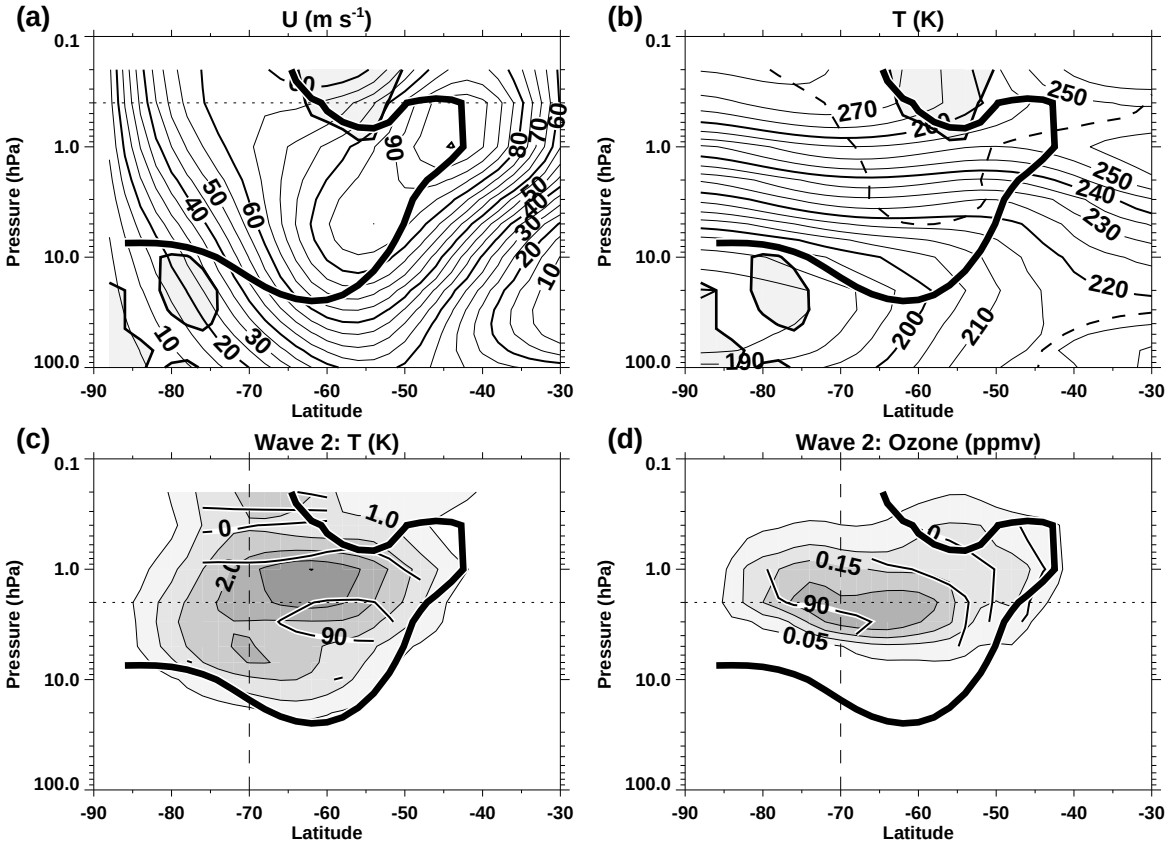

Figure 8: Wave 2 structure, July 1998, 1.72 day period, as a function of latitude and pressure. The heavy dark line is the critical line. (a) zonal mean zonal wind (m s^{-1}). Shaded region is where the zonal mean pv gradient, $\bar{q}_y$, is negative. Dotted reference line at 0.4 hPa (b) zonal mean temperature (K). Dashed line is where the horizontal temperature gradient is zero. Shaded region is where $\bar{q}_y$, is negative. (c) temperature wave amplitude (K, shaded contours, contour interval 0.5 K) and phase (degrees, black lines, contour interval 45°). (d) ozone wave amplitude (ppmv, shaded contours, contour interval 0.05 ppmv) and phase (degrees, black lines, contour interval 45°). Reference lines at 70°S and 2 hPa in (c) and (d).

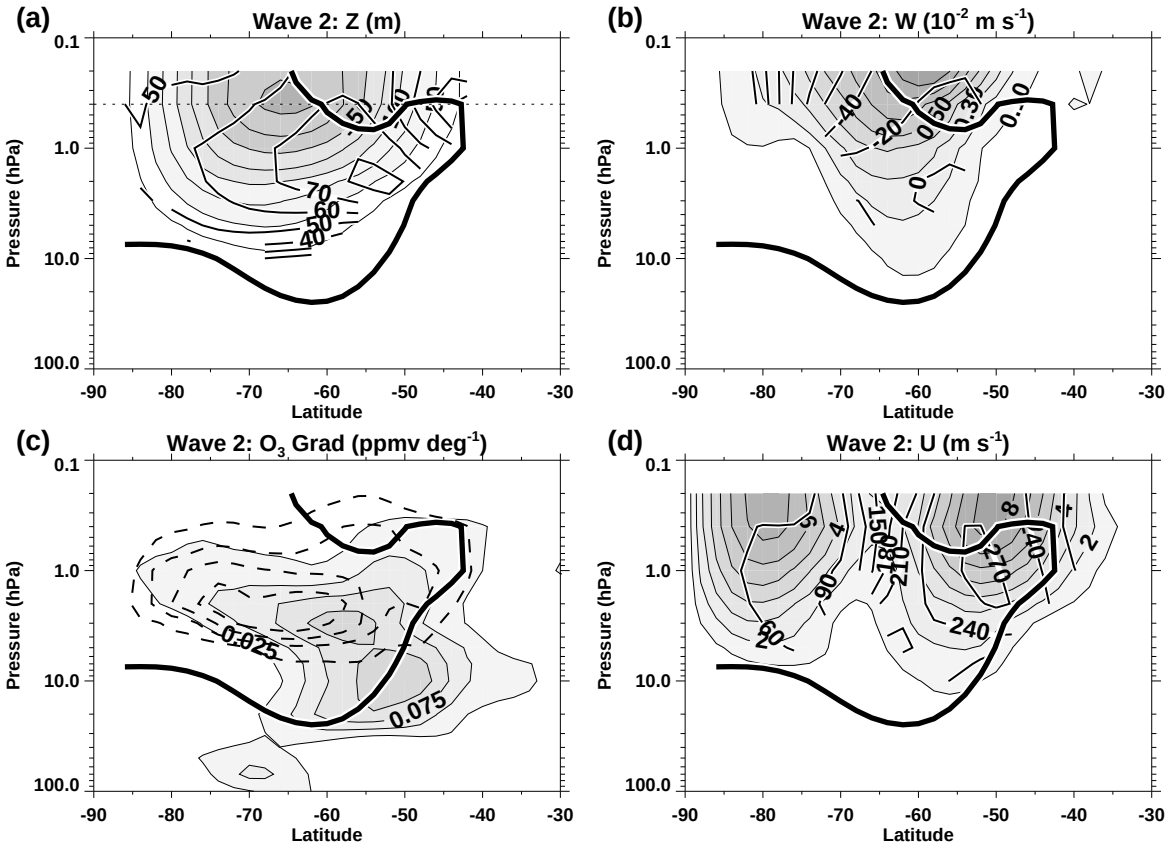

Figure 9: Wave 2 structure, July 1998, 1.72 day period, as a function of latitude and pressure. The heavy dark line is the critical line. (a) height wave amplitude (m, shaded contours, contour interval 10 m, maximum contour is 80 m) and phase (degrees, black lines, contour interval 10°). Dotted reference line at 0.4 hPa (b) vertical Velocity amplitude (x10^{-2} m s^{-1}, shaded contours, contour interval 0.1 x10^{-2} m s^{-1}) and phase (degrees, black lines, contour interval 20°). (c) mean latitudinal ozone gradient (ppmv deg^{-1}, shaded contours, contour interval 0.025 ppmv deg^{-1}) and ozone wave amplitude (dashed lines) taken from fig. 8(d). (d) zonal wind amplitude (m s^{-1}, shaded contours, contour interval 1 m s^{-1}) and phase (degrees, black lines, contour interval 30°).

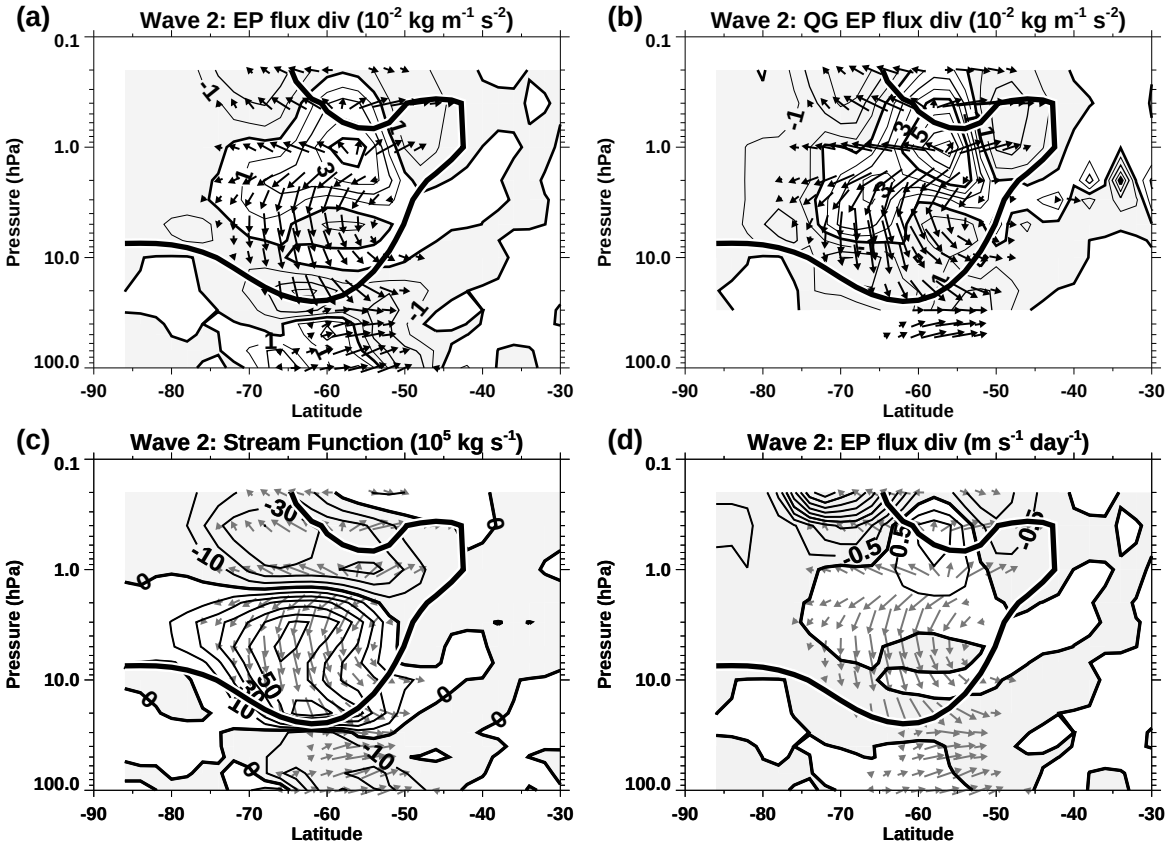

Figure 10: Wave 2 structure, July 1998, 1.72 day period, as a function of latitude and pressure. The heavy dark line is the critical line. (a) EP flux divergence (x10^{-2} kg m^{-1} s^{-2}), negative values are shaded, contour interval 1x10^{-2} kg m^{-1} s^{-2} and EP flux vectors. (b) same as (a) except calculated from heights using quasi-geostropic approximation. (c) wave induced mass stream function (x10^5 kg s^{-1}, contours, negative values are shaded, contour interval 10x10^5 kg s^{-1}) and EP flux vectors from (a). (d) zonal mean wind forcing (m s^{-1} day^{-1}, negative values are shaded, contour interval 0.5 m s^{-1} day^{-1}) and EP flux vectors from (a).

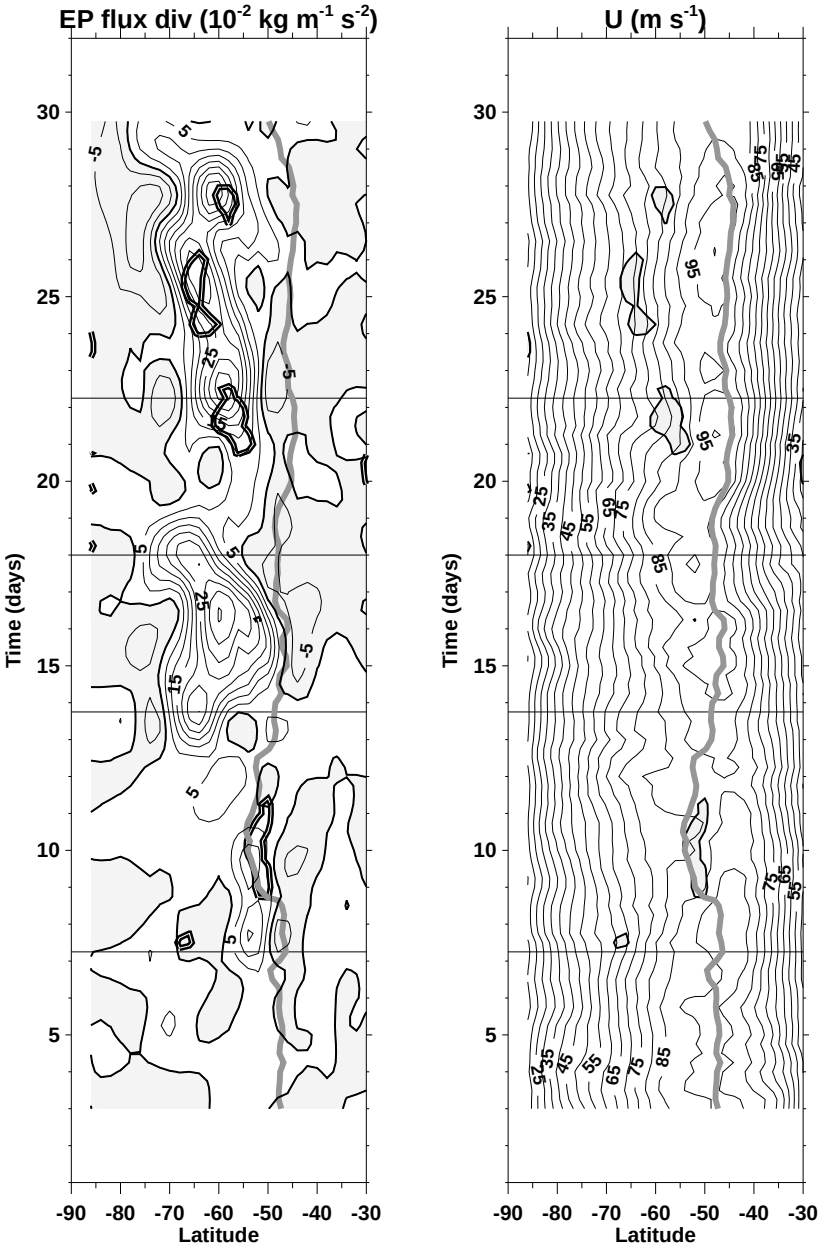

Figure 11: Time latitude plots at 2 hPa for July 1998: (a) band pass filtered EP flux divergence (x10^{-2} kg m^{-1} s^{-2}), contour interval 5x10^{-2} kg m^{-1} s^{-2}, negative values are shaded, negative $\bar{q}_y$ regions double outlined. (b) zonal mean zonal wind (m s^{-1}), contour interval 5 m s^{-1}, negative $\bar{q}_y$ regions shaded. Thick gray line is the 0.58 day^{-1} critical line. The 4 horizontal lines correspond to the 4 times shown in fig. 13

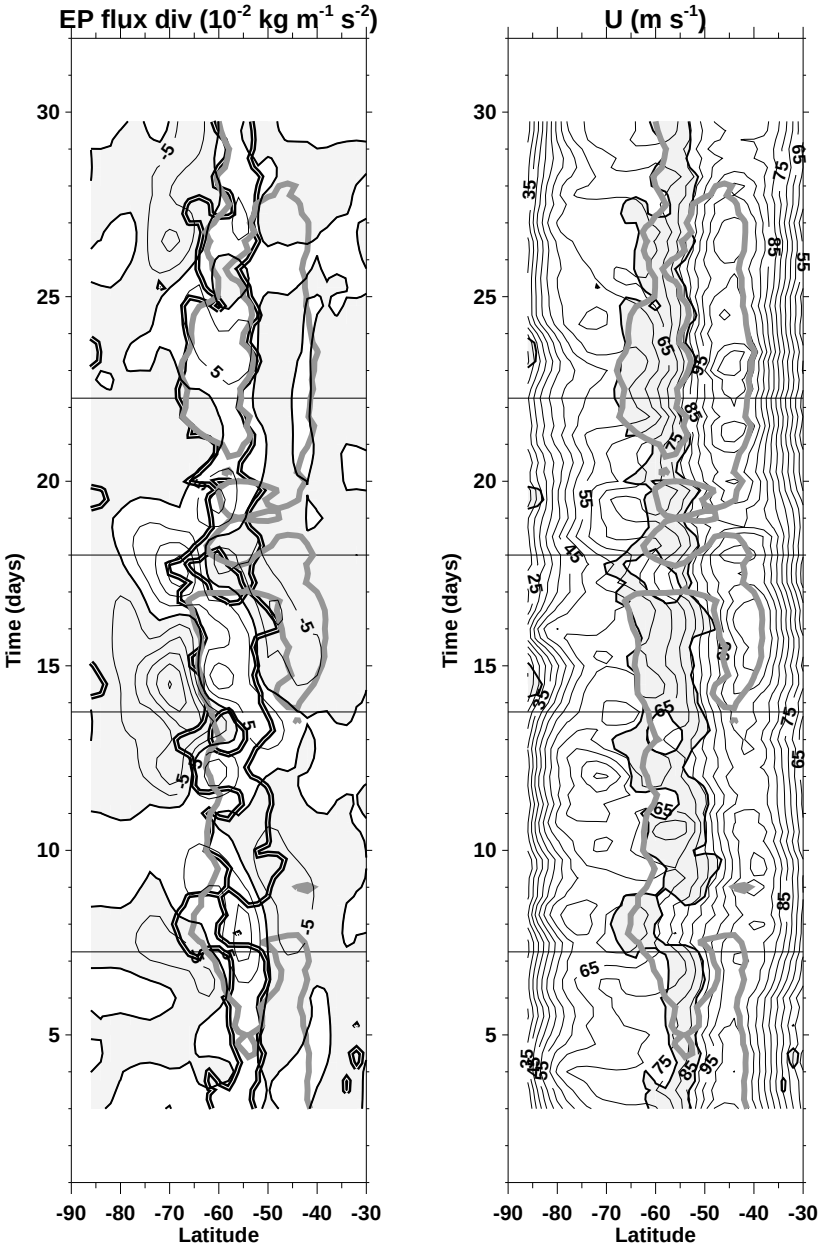

Figure 12: As in fig. 11 for 0.4 hPa

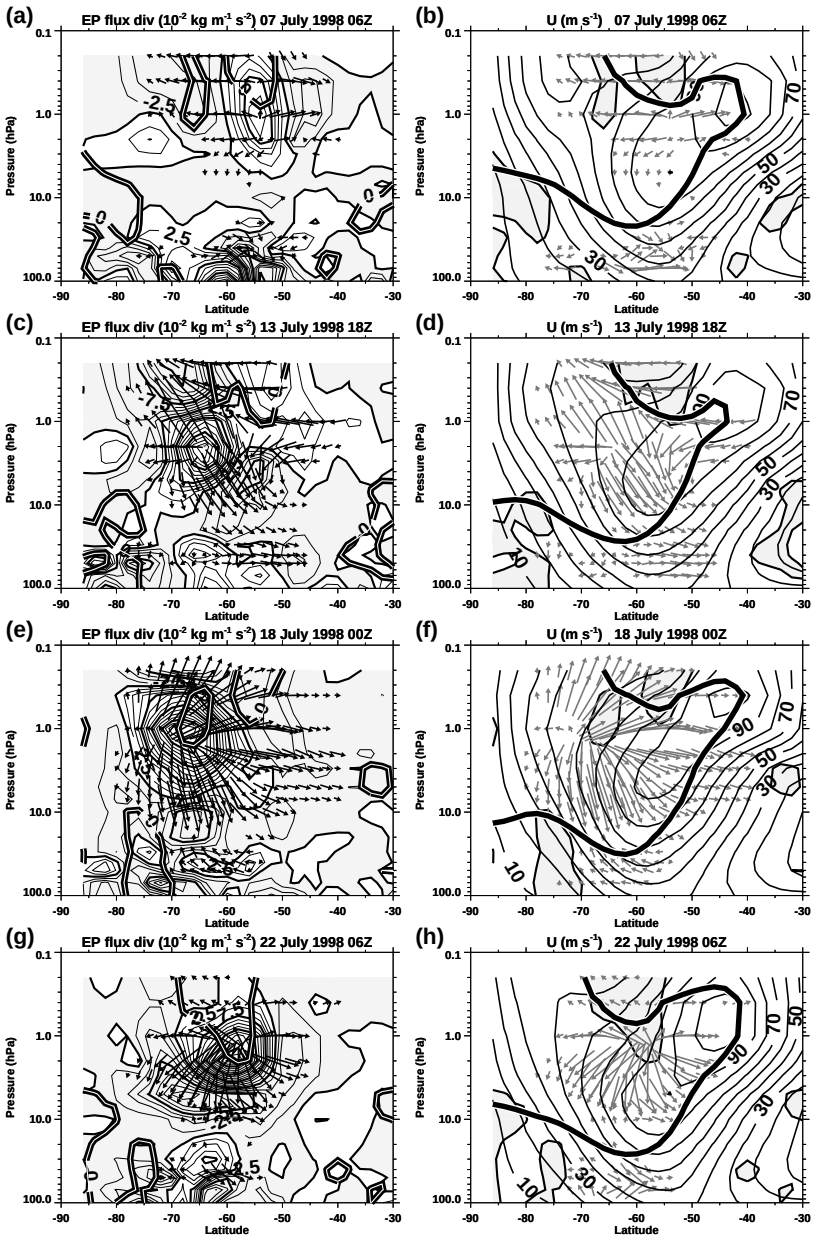

Figure 13: Plots of EP flux divergence (left, contour interval 2.5x10^{-2} kg m^{-1} s^{-2}, negative values are shaded) and zonal mean zonal wind (right, contour interval 10 m s^{-1}) at four times during July 1998. EP flux vectors are scaled 40% smaller than in fig. 10. The heavy line on the right is the 1.72 day critical line. Negative $\bar{q}_y$ regions are shaded on the right and $\bar{q}_y = 0$ are double lines on the left.

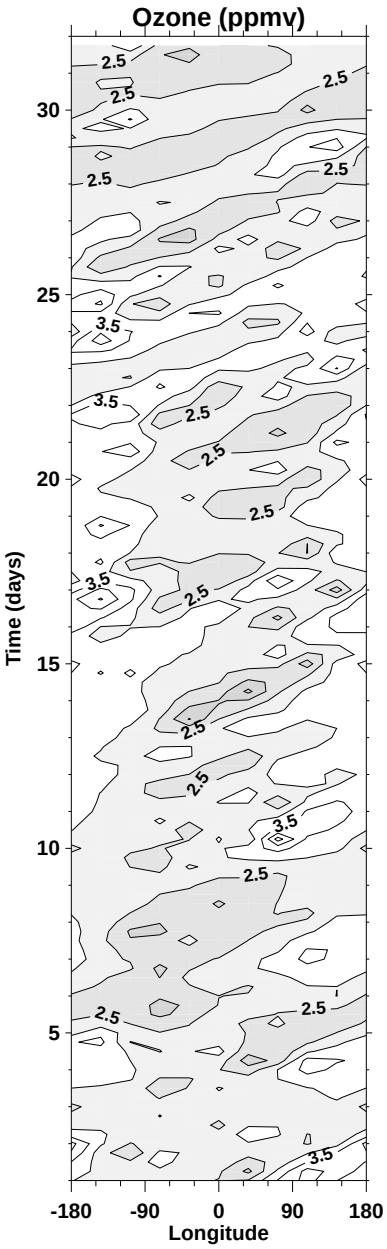

Figure 14: Longitude time plot of POAM ozone (ppmv) at an average latitude of 68°S and 2 hPa for July 1998. Contour interval is 0.5 ppmv. Lower ozone values are shaded.

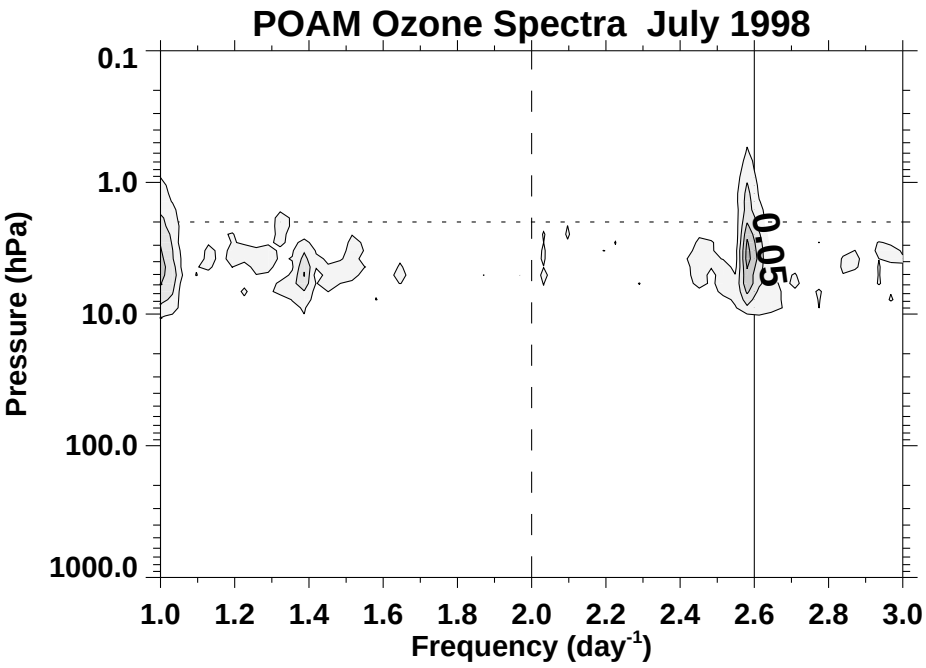

Figure 15: POAM ozone power spectra (ppmv) for July 1998 as a function of frequency and pressure, contour interval 0.05 ppmv.